JGR Space Physics

RESEARCH ARTICLE
10.1029/2019JA026961

Low Electron Temperatures Observed at Mars by MAVEN on Dayside Crustal Magnetic Field Lines

Shotaro Sakai[1], Thomas E. Cravens[2], Laila Andersson[3], Christopher M. Fowler[3,4], David L. Mitchell[4], Christian Mazelle[5], Edward M. B. Thiemann[3], Francis G. Eparvier[3], David A. Brain[3], and Kanako Seki[1]

[1]Department of Earth and Planetary Science, Graduate School of Science, University of Tokyo, Tokyo, Japan, [2]Department of Physics and Astronomy, University of Kansas, Lawrence, KS, USA, [3]Laboratory for Atmospheric and Space Physics, University of Colorado Boulder, Boulder, CO, USA, [4]Space Science Laboratory, University of California, Berkeley, CA, USA, [5]IRAP, Université de Toulouse, CNRS, CNES, UPS-OMP, Toulouse, France

Key Points:
- At high altitudes, the electron temperature is lower for the crustal-field region than for the IMF-dominated draped regions
- The low temperatures for the crustal-field region are due to a heat transport along the field lines between lower and upper atmosphere
- Kinetic effects such the magnetic mirror and the ambipolar electric field may affect the heat transport along crustal magnetic field lines

Correspondence to:
S. Sakai,
shotaro@eps.s.u-tokyo.ac.jp

Citation:
Sakai, S., Cravens, T. E., Andersson, L., Fowler, C. M., Mitchell, D. L., Mazelle, C., et al. (2019). Low electron temperatures observed at Mars by MAVEN on dayside crustal magnetic field lines. *Journal of Geophysical Research: Space Physics*, *124*, 7629–7637. https://doi.org/10.1029/2019JA026961

Received 21 MAY 2019
Accepted 7 AUG 2019
Accepted article online 23 AUG 2019
Published online 5 SEP 2019

Abstract The ionospheric electron temperature is important for determining the neutral/photochemical escape rate from the Martian atmosphere via the dissociative recombination of O_2^+. The Langmuir Probe and Waves instrument onboard MAVEN (Mars Atmosphere and Volatile EvolutioN) measures electron temperatures in the ionosphere. The current paper studies electron temperatures in the dayside for two regions where (1) crustal magnetic fields are dominant and (2) draped magnetic fields are dominant. Overall, the electron temperature is lower in the crustal-field regions, namely, the strong magnetic field region, which is due to a transport of cold electrons along magnetic field lines from the lower to upper atmosphere. The electron temperature is also greater for high solar extreme ultraviolet conditions, which is associated with the local extreme ultraviolet energy deposition. The current models underestimate the electron temperature above 250-km altitude in the crustal-field region. Electron heat conduction associated with a photoelectron transport in the crustal-field regions is altered due to kinetic effects, such the magnetic mirror and/or ambipolar electric field because the electron mean free path exceeds the relevant length scale for electron temperature. The mirror force can affect the electron and heat transport between low altitudes, where the neutral density and related electron cooling rates are the greatest, and high altitudes, while the ambipolar electric field decelerates the electron's upward motion. These effects have not been included in current models of the electron energetics, and consideration of such effects on the electron temperature in the crustal-field region should be considered for future numerical simulations.

1. Introduction

The Mars Atmosphere and Volatile EvolutioN (MAVEN) spacecraft (s/c) has observed the ionosphere of Mars since November 2014. Describing and explaining how the electron temperature (T_e) in the ionosphere varies with location and with solar conditions (Jakosky et al., 2015) is important because T_e significantly affects the dissociative recombination rate of O_2^+ ions, which is a key pathway for photochemical escape of neutral oxygen (Ergun et al., 2015; Lillis et al., 2015). A key goal of the MAVEN mission is to characterize the escape of atmospheric gas to space, and thus, knowledge of T_e is important.

The only in situ measurements of plasma temperatures in the ionosphere prior to the MAVEN mission were provided by the two Viking landers in 1976. The Retarding Potential Analyzer onboard Viking 1 measured electron temperatures above 200 km, and the data showed three electron populations, that is, (1) thermal electrons, (2) photoelectrons, and (3) electrons of solar wind origin, with temperatures of about 3,000, 30,000, and 200,000 K above 250 km, respectively (Hanson & Mantas, 1988). The amount of T_e data and suprathermal electron data has dramatically increased since MAVEN arrived at Mars. The Langmuir Probe and Waves (LPW) instrument onboard MAVEN measures electron temperatures and densities (Andersson et al., 2015). Ergun et al. (2015) presented altitude profiles of electron temperature obtained during the MAVEN deep dip campaign in April 2015, during which periapsis altitude was as low as 130 km (Jakosky et al., 2015). The LPW data showed that the electron temperature increases with altitude from ≈600 K at 130 km to 980 K at 200 km. The LPW instrument has a lower temperature limit of ≈500 K, and so temperatures reported close to 500 K might actually be lower than this (Ergun et al., 2015). Ergun et al.

(2015) also showed that the electron temperature rapidly increases from ≈800 to ≈2,800 K as altitude increases from 180 to 300 km.

Suprathermal electrons, which can heat thermal electrons via Coulomb collisions, have also been observed at Mars by the Magnetometer and Electron Reflectometer (MAG/ER) instrument onboard the Mars Global Surveyor (MGS) s/c (Liemohn et al., 2003, 2006; Mitchell et al., 2000) and the Electron Spectrometer (ELS) from the Analyzer of Space Plasmas and Energetic Atoms (ASPERA-3) onboard the Mars Express (MEX) s/c (Coates et al., 2011; Frahm et al., 2006; Lundin et al., 2004). The Solar Wind Electron Analyzer (SWEA) instrument onboard MAVEN (Mitchell et al., 2016; Sakai et al., 2015, 2016) has been also measured the suprathermal electrons in recent years.

Past observations have shown that the ionospheric electron characteristics are influenced by the crustal magnetic field (e.g., Andrews et al., 2013, 2015; Fang et al., 2017; Withers et al., 2005). The ionosphere of Mars contains both solar wind draped magnetic fields and local crustal magnetic fields depending on the geographical locations (Acuña, 1998), although Mars currently has no significant global intrinsic magnetic field. The crustal magnetic fields are in both open (i.e., cusps) and closed field lines (Brain et al., 2007; Xu et al., 2017), and the configuration is time-dependent. In both cases the magnetic field provides good connectivity between high and low altitudes in the ionosphere, that is, between ~100- and 500-km altitudes, in comparison with the largely horizontal fields, namely, the draped magnetic field of solar wind origin (Bertucci et al., 2003; Brain et al., 2003). Flynn et al. (2017) showed that the electron density is higher (e.g., Andrews et al., 2013, 2015) and temperature is lower in the dayside ionosphere of the crustal-field regions above 200 km. They qualitatively anticipated that processes associated with plasma transport lead to the observed anticorrelation of electron densities and temperature in the crustal-field region at Mars (e.g., Schunk & Nagy, 2009).

Several numerical models also have reproduced the electron temperatures observed by Viking and MAVEN with varying degrees of success. Past simulations suggested that the heating by solar radiation was not sufficient, instead that external heat fluxes at the "top" of the ionosphere are required in order to explain the Viking observations (Chen et al., 1978; Choi et al., 1998; Cravens et al., 1980; Johnson, 1978; Matta et al., 2014; Rohrbaugh et al., 1979; Singhal & Whitten, 1988). Matta et al. (2014) showed that topside heat fluxes of 1.5×10^{10} eV · cm^{-2} · s^{-1} for electrons and 2×10^{7} eV · cm^{-2} · s^{-1} for ions are needed to match the Viking data. Sakai et al. (2016) were able to reproduce the high topside electron temperatures (e.g., 3,000 K at 300-km altitude) observed by MAVEN without invoking a topside heat flux when magnetic field topologies consistent with the measured magnetic field were adopted, namely, mainly draped and horizontal. However, the electron temperatures were lower when the radial/vertical magnetic field lines are considered due to efficient heat transport from higher to lower altitudes. This suggested that the modeled electron temperature should be lower than the observations in the crustal-field region, but the transport mechanism is not clear.

In the current paper, based on MAVEN data analysis, we show that the reason why the current models cannot accurately predict electron temperature in the high altitude of crustal-field region is the neglect of kinetic effects, such as the magnetic mirror force and ambipolar electric field, on electron heat transport in the presence of crustal fields. The current paper also confirms the Flynn et al. (2017) conclusion just stated.

2. MAVEN LPW

The MAVEN LPW in its Langmuir Probe (LP) mode measures current-voltage (I-V) characteristics, from which the local electron density, temperature, and s/c potential are derived (Andersson et al., 2015; Ergun et al., 2015). In its wave mode, LPW can detect plasma waves that can heat ions, resulting in atmospheric escape (Andersson et al., 2015; Ergun et al., 2006; Fowler et al., 2017). The electron temperatures obtained from the LP mode are the subject of the current paper. The LP sensor has two independent cylindrical probes that are 0.635 cm in diameter and 40 cm long. The probes are situated 7.1 m from the s/c main body. The LP instruments measure the electrical current collected by the impinging plasma particles by sweeping the probe-biased voltages, normally with 128 steps, for a voltage range that depends on the s/c altitude and local plasma conditions. At periapsis, where cold electrons of <1 eV (≈12,000 K) dominate, the LP instrument is typically operated with a sweep range of ± 5 V, a sweep duration of 1–4 s, and at a cadence of 1–2 sweeps per 4 s. The local electron density and temperature are derived from each current-voltage curve using an enhanced fitting process based on those presented by, for example, Ergun et al. (2015).

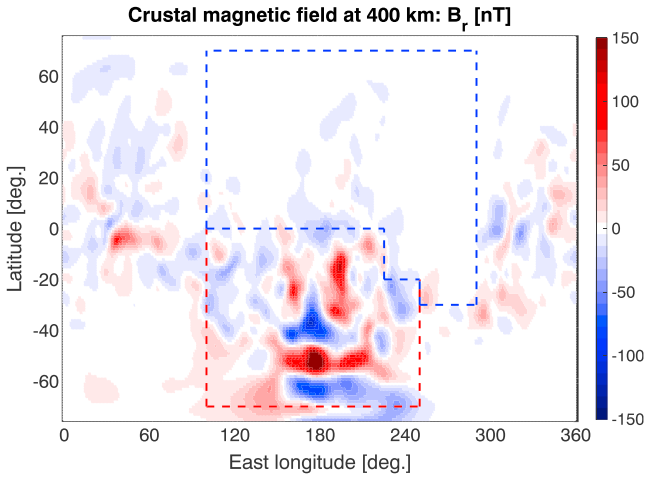

Figure 1. The radial component of the crustal magnetic field at 400 km based on Cain et al. (2003) is shown on the Martian map. Areas surrounded by red and blue dashed lines denote the crustal-field region and the draped region, respectively.

3. MAVEN Orbits Used in the Study: Data Selection

The dependence of electron temperatures on magnetic field configuration is studied in the current paper. Mars has no significant global intrinsic magnetic field, but it does have localized intrinsic crustal magnetic fields (Acuña, 1998; i.e., cusp or closed) at some geographic locations, concentrated mainly in the southern hemisphere. We investigate the electron temperature, photoelectron flux, and magnetic characteristics in two geographical regions: (1) the crustal magnetic field region and (2) the draped magnetic field region. We use the geographical position of MAVEN (i.e., latitude and longitude) to define whether the s/c is sampling a crustal field region or in a draped magnetic field region. Figure 1 shows a map of the radial component of crustal magnetic field (Br). We use the dayside data taken at an altitude below 500 km and solar zenith angle less than 70°. The LPW data in the time period from April 2015 to March 2018 are statistically investigated, which covers all seasons of Mars.

Our criteria for defining the dayside crustal region are (1) a latitude range of 70°S to 0°N and (2) a longitude range of 100° to 250° (cf. Connerney et al., 2005) except for the area of 225° < lon. < 250° and 20°S < lat. < 0°N, which is used for the draped region. The crustal-field region used is also shown in an area surrounded by red dashed lines of Figure 1.

For the draped magnetic field regions on the dayside in our study we used the following criteria: (1) a latitude range of 30°S to 70°N and (2) a longitude range of 100 to 280° except for the areas of 100° < lon. < 225° and 20°S < lat. < 0°, and 225° < lon. < 250° and 30°S < lat. < 20°S, which are used for the crustal-field region. This region is also shown in Figure 1 as the area surrounded by blue dashed lines.

4. Electron Temperatures Measured by LPW

4.1. Temperature Dependence on Magnetic Field Topology: Crustal-Field Region Versus Draped-Field Region

The electron temperature measured by LPW at 200-km altitude is typically about 1,000 K, but T_e dramatically increases above 200 km, and almost reaches 3,000 K at an altitude of about 400 km (e.g., Ergun et al., 2015; Flynn et al., 2017). The LPW instrument is designed to measure the high densities (10–10^5 cm^{-3}) and low temperatures (< 1 eV or ≈12,000 K) that characterize the Martian ionosphere (Andersson et al., 2015). When the temperature is larger than ≈1 eV (the suprathermal portion of the distribution contributes to the cold core distributions) LPW cannot resolve the hot temperature. Electron temperatures for the crustal-field region and the draped-field region are compared in this section. Figure 2 shows T_e distributions (grey dots) in crustal- (panel a) and draped-field (panel c) regions.

The electron temperatures observed by MAVEN have the same trend reported by previous studies (e.g., Ergun et al., 2015). Figures 2b and 2d show histograms of electron temperature distribution every 125 K at 275–325 km for the crustal- (light pink; panel b) and draped-field (light blue; panel d) regions. One can obviously find that the temperature is higher for the draped-field case from the histograms (Figures 2b and 2d). The mean temperature is ≈2,400 K for the crustal-field region and ≈3,400 K for the draped-field region. The scatter in the temperatures is particularly large for the draped-field region. The histograms indicate that the difference is mainly in the high-temperature "tail" present in the draped-field histogram, which causes the temperature scatter for the draped-field region. The ratio of $T_e \geq 4{,}000$ K to the population is ≈3% in the crustal-field region and ≈14% in the draped-field region. The high-temperature component could originate from the solar wind or magnetosheath because the draped field is originally the solar wind magnetic field. These results support the Flynn et al. (2017) conclusions. Ergun et al. (2015) estimated a range of scatter of the LPW electron temperatures observed by LPW in the 300- to 500-km altitude range of 2,500 to 3,500 K with a mean temperature of 3,130 K. The spread was less for altitudes lower than 300 km (see Figure 4 of Ergun et al.).

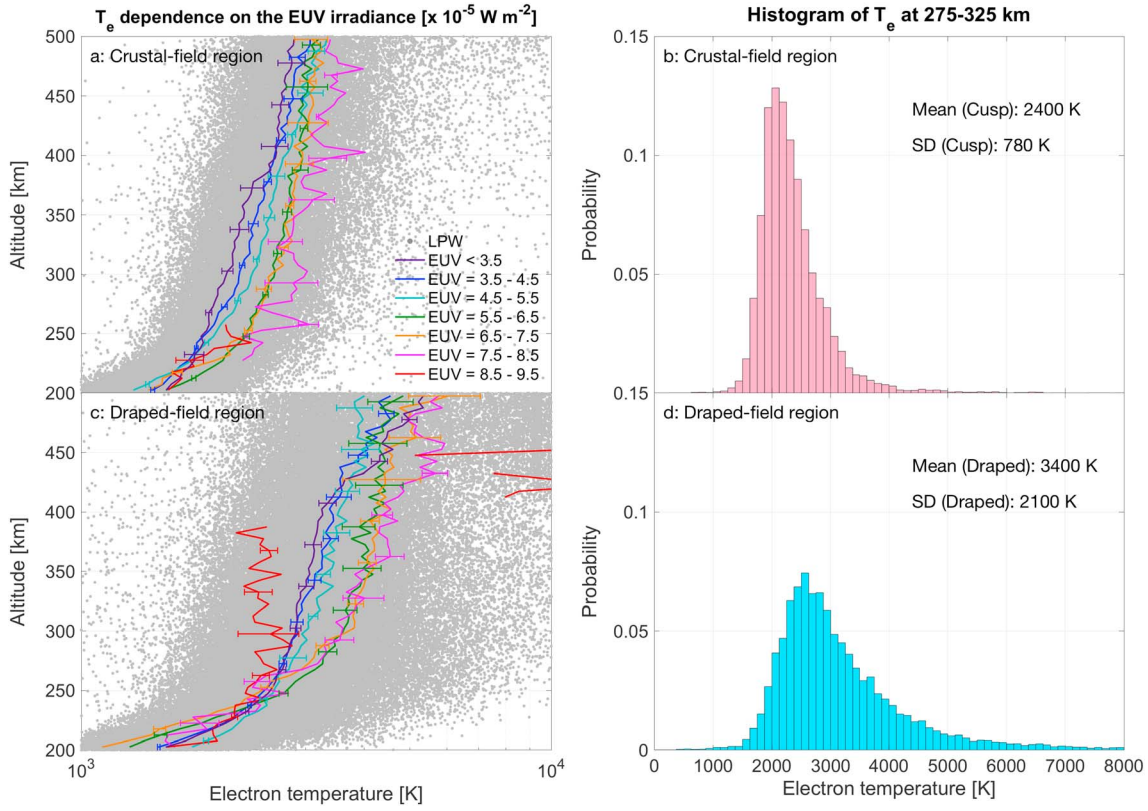

Figure 2. Scatter plot of ionospheric electron temperatures for (a) crustal-field region and (c) draped-field region observed by Mars Atmosphere and Volatile EvolutioN (MAVEN) Langmuir Probe and Waves (LPW). The colored lines of panels a and c show the median of electron temperature in each solar extreme ultraviolet irradiance bin along with error bars of the standard error. The histograms of temperatures for (b) crustal- (light pink) and (d) draped-field region (light blue) are also shown along with the mean value and standard variation (SD).

The solar extreme ultraviolet (EUV) radiation influences the ionospheric energy transport. The colored lines of Figures 2a and 2c show the electron temperature at each EUV irradiance level. Note that daily-averaged EUV irradiances (17–22 nm) are used to sort the data. We adopt the daily-averaged Flare Irradiance Spectral Model-Mars (FISM-M; Chamberlin et al., 2007; Thiemann et al., 2017), which determines irradiances based on the MAVEN EUV Monitor (Eparvier et al., 2015) Level 3 data product (Thiemann et al., 2017) for the EUV irradiances and gives the spectral irradiances at a 1-min cadence and also daily averages.

The measured electron temperature is higher when EUV irradiances are higher in both crustal and draped-field regions except for the very highest EUV case (which we do not understand), and it is consistent with results of the EUV deposition, which takes place in the ionosphere below 210-km altitude (Peterson et al., 2018). It suggests that the high solar irradiance raises the electron temperature. In contrast, the temperature is still lower for the crustal-field region at the same EUV irradiance level. Note that the oscillation of red lines is due to the small number of samples in this EUV range.

4.2. Dependence on Magnetic Field and on Suprathermal Electrons

The crustal magnetic field should affect the electron temperature distribution because forces interacting on crustal-field lines are different from those on draped field lines. Figure 2 of this paper and Flynn et al. (2017) both showed that the temperatures are lower for the crustal-field region at high altitudes. Two selected regions in this study support this, and the magnetic field trends are presented in Figure 3. The figure shows mean temperature for a local magnetic field independent of the region, and this suggests that the strong magnetic field is associated with lower temperature. One possible explanation for low electron temperature in the crustal-field region is the magnetic mirror force on electrons, which is larger in the crustal-field region

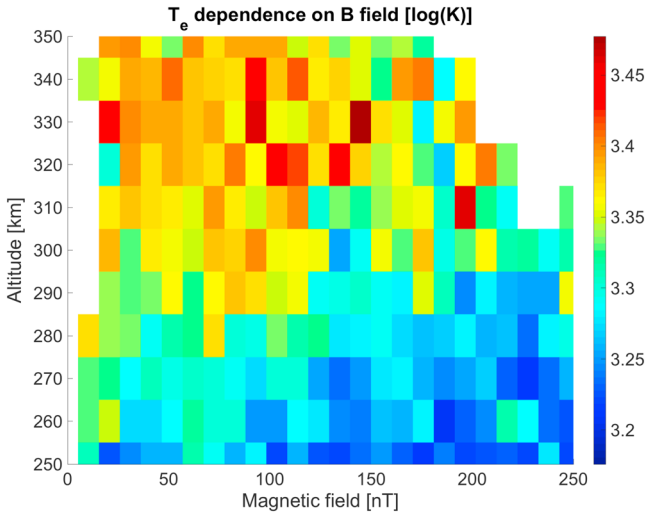

Figure 3. The dependence of electron temperature on the magnetic field strength as a function of altitude.

than in the draped-field region. The magnetic mirror force could be a driver of electron transport along the field line from low where the colder electrons than 1 eV (≈12,000 K) are dominant to high altitude, facilitating the electron cooling at high altitude.

Photoelectron distributions are also important for determining the electron temperature in the ionosphere because they heat the cold electrons by a few eV via Coulomb collisions, transferring energy from solar photons to the electron gas. The relationship between suprathermal electrons including photoelectrons and electron temperature are investigated with MAVEN data. Sakai et al. (2015) presented comparisons between modeled suprathermal electron fluxes and fluxes measured by the SWEA instrument. Figures 4a shows electron flux measured by SWEA integrated over energy for an altitude of around 300 km for all energies. Note that the SWEA instrument measures electron fluxes for energies between 3 eV and 4.6 keV (Mitchell et al., 2016). The area surrounded by black dashed lines shows the crustal-field region in this study.

The mean flux integrated over all energy bins is mostly the same in both the crustal-field and draped-field region (Figure 4a). Note that fluxes integrated over all energy bins are dominated by fluxes below 20 eV (e.g., Sakai et al., 2015; Xu et al., 2017), which are expected to mainly be photoelectrons and not solar wind electrons (Liemohn et al., 2003; Sakai et al., 2015), and such suprathermal electrons are effective for the electron heating. Figure 4b shows examples of energy flux spectra observed by SWEA in both crustal-field (blue) and draped-field (green) regions. The shape of the electron energy spectra does not change much, but quantitatively, the flux is slightly greater in the crustal-field region than in the draped-field region. However, the electron temperature that LPW observed at this time is lower in the crustal-field region, that is, T_e ≈2,000 K in the crustal-field region and ≈2,400 K in the draped-field region at 300-km altitude. This suggests that the lower electron temperatures measured in the crustal-field regions cannot solely be explained by lower suprathermal electron (i.e., photoelectron) fluxes and might be related to the ambipolar electric field or some other factor. Note that the solar zenith angle was close to ≈64° in both cases and EUV irradiances were ≈2.4 × 10^{-5} W/m^2 and ≈2.8 × 10^{-5} w/m^2 in the crustal-field region and draped-field region, respectively.

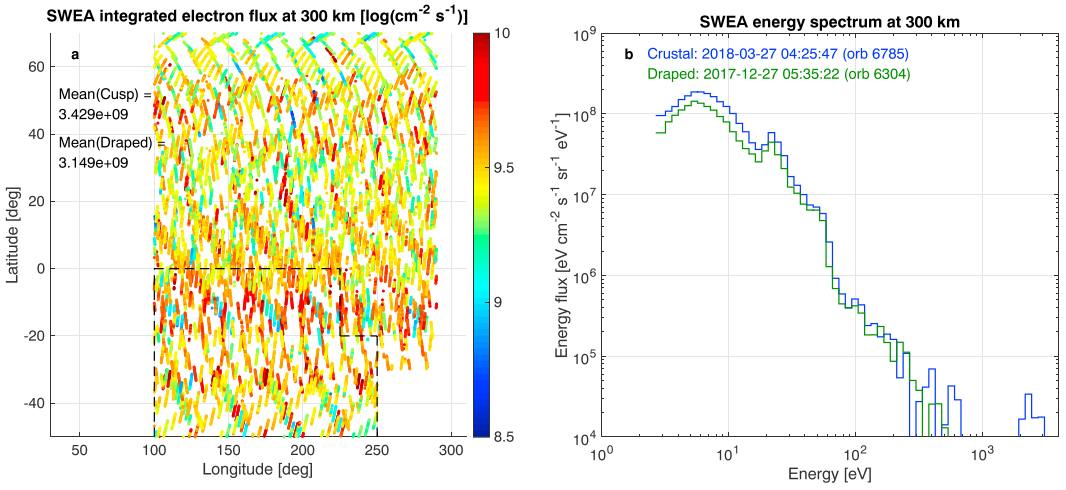

Figure 4. (a) The omnidirectional electron fluxes integrated over energies for all energy bins observed by Solar Wind Electron Analyzer (SWEA) when Mars Atmosphere and Volatile EvolutioN (MAVEN) was between 275- and 325-km altitude. The dashed box indicates the crustal-field region. (b) Examples of the SWEA energy spectrum observed in the crustal-field region (blue) and draped-field region (green). MAVEN passed through the crustal-field region at 4:25 on 27 March 2018 and the draped-field region at 5:35 on 27 December 2017.

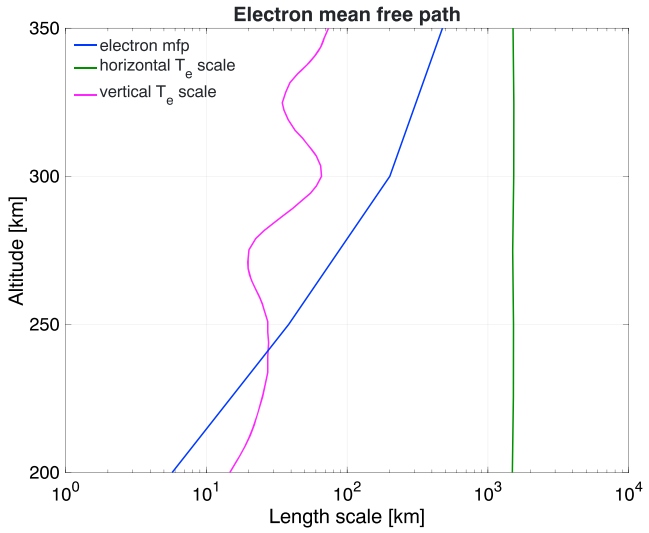

Figure 5. Electron mean free path (blue) is shown as a function of altitude. Typical length scales for horizontal (green) and vertical (magenta) T_e variations are shown for comparison.

5. Discussion

5.1. Low Electron Temperatures in the Crustal-Field Region

Electron temperatures measured by LPW on the dayside were typically lower for the crustal-field region than for the draped-field region at altitudes between 200 and 400 km (Figure 2, and also see Flynn et al., 2017). Given the modeling results shown by Sakai et al. (2016) or by Matta et al. (2014), perhaps this is not entirely surprising. These authors solved the electron energy equation, which includes photoelectron heating, electron-neutral and ion cooling, and heat conduction, subject to different assumptions on the magnetic field topology. Sakai et al. (2016) found that for mainly horizontal (draped) magnetic field lines, model temperatures at altitudes higher than 200 km agreed with LPW data reasonably well ($T_e \approx 3000$ K; Figures 2c and 2d of current paper). However, when the magnetic field was mainly radial/vertical, allowing efficient heat transport from higher to lower altitudes, the calculated temperature above 200 km was much lower ($T_e \approx 1{,}000$ K), and less than the measured temperatures ($T_e \approx 2{,}000$ K; see Figures 2a and 2b of current paper). Similar results were obtained by Matta et al. (2014). To summarize this, current models underestimate the electron temperatures inside crustal-field regions, as compared to MAVEN observations (i.e., the current paper and Flynn et al., 2017).

The current theoretical treatment of the electron energetics for the crustal field regions of Mars is missing something. One possible problem with the standard heat conduction formulation (cf., Schunk & Nagy, 2009) for the Martian crustal-field ionosphere is that the electron collisional mean free path (mfp), λ_{mfp}, for higher altitudes is comparable to, or exceeds, the scale-length of the temperature gradient ($L \approx T_e/|dT_e/ds| \approx 50$ km). That is, the standard heat conduction formulation is not adequate in this case. For draped magnetic fields at Mars, or any field configuration that is largely horizontal, the conduction length scale $L \approx R_M/2 \approx 1{,}500$ km where R_M is the radius of Mars, which should make the conduction formalism more appropriate. However, for crustal field regions, the field configurations are more "confined" than for the draped case and have larger radial/vertical components. Note that everywhere in the part of the ionosphere observed by MAVEN ($z > 140$ km or so) the electron gyrofrequency ($\Omega \approx 1{,}000\ s^{-1}$ for a 10 nT field) exceeds the collision frequency ($\nu_{en} \approx 100\ s^{-1}$ at the ionospheric peak). The heat flux in the direction, s, along the magnetic field is given by $F = -K_e\,(dT_e/ds)$ with conductivity coefficient (Rees, 1989):

$$K_e \approx (\zeta/3) n_e k_B \langle v_e \rangle \lambda_{mfp}$$

where n_e is the electron density, k_B is Boltzmann's constant, $\langle v_e \rangle$ is the random electron speed (i.e., the thermal speed, $\langle v_e \rangle = [k_B T_e/m_e]^{1/2}$), and ζ is a numerical constant of order unity. For $T_e \approx 1{,}500$ K, the electron random velocity $\langle v_e \rangle$ is ≈150 km/s.

When the dominant collision process is electron Coulomb collisions with electrons and ions (i.e., collision frequency of $\nu_{ee} = \nu_{ei} = bn/T^{3/2}$ where $b \approx 54$ for n in cgs units—cf., Schunk & Nagy, 2009), the mfp is $\lambda_{mfpee} \approx \langle v_e \rangle/\nu_{ee}$ and one obtains the standard Spitzer conductivity: $K_e = [(\zeta k_B^2)/(bm_e)]T_e^{5/2}$. If electron-neutral collisions also take place, then the mfp is $\lambda_{mfp}^{-1} = \lambda_{mfpee}^{-1} + \lambda_{mfpen}^{-1}$. The electron-neutal mfp is represented by $\lambda_{mfpen} \approx \langle v_e \rangle/\nu_{en}$ with collision frequency $\nu_{en} \approx cn_n$, where n_n is the neutral number density in cgs units and $c \approx 10^{-8}$ cm^3/s is a coefficient depending on target species and other parameters (Cravens, 1997).

Figure 5 shows the electron mean free path versus altitude using typical densities measured by MAVEN (Table 2 from Cravens et al., 2017). Relevant length scales for T_e spatial variations can be estimated from $L \approx T_e/(dT_e/ds)$, where s is horizontal distance or altitude. For draped-field regions the length scales are greater than the mfp and a standard conductivity approach should be valid (i.e., Sakai et al., 2016). However, for crustal regions, the mfp exceed the relevant length scales for altitudes above 200 km. A theoretical approach has not, to our knowledge, been developed that would handle this situation, at least for Mars, and takes into account possible processes such as magnetic mirroring, polarization electric fields,

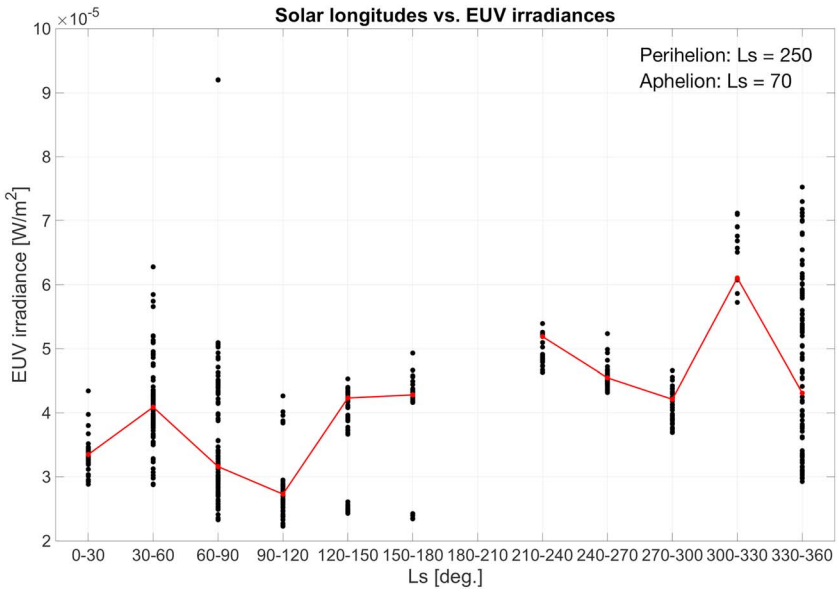

Figure 6. The dependences of the solar longitude on the extreme ultraviolet (EUV) irradiances are plotted every 30°. The black dots are the EUV irradiances based on the Mars Atmosphere and Volatile EvolutioN (MAVEN) observations, and the red lines denote the median of EUV irradiances every 30°.

and pitch-angle scattering. Note that the mfp is actually dominated by λ_{mfpee} above 200-km altitude because the electron-neutral collision frequency is quite small.

The transport of photoelectrons, as well as thermal electrons, is also affected by the above limitations, especially in the crustal-field region (e.g., Liemohn et al., 2003). The SWEA instrument observed substantial low energy electron fluxes at higher altitudes that probably were created deeper in the ionosphere by the photoionization of neutrals (Figure 4b). The radial transport of electrons along crustal field lines should be affected by (1) the magnetic mirror force and (2) the ambipolar electric field force. The magnetic mirror force can move electrons from lower ionosphere where cold electrons are dominant to upper atmosphere, contributing to the electron cooling at higher altitudes. The ambipolar electric field decelerates the electron's upward motion. The balance between the magnetic mirror force and ambipolar electric field is important in determining the electron temperature in the crustal-field region.

5.2. Influence of the Solar Longitude on Electron Temperature

The electron temperature depends on the EUV irradiances and is higher for high EUV levels (Figure 2). The EUV irradiances might be affected by the solar longitude (Ls). Figure 6 shows the Ls dependence on EUV irradiances for 3 years from April 2015 to March 2018. Note that the Ls is plotted every 30°. The EUV irradiances tend to be low around the aphelion (Ls = 70°) and high around the perihelion (Ls = 250°). It means that the EUV irradiances vary with Ls. The EUV irradiances are high when Mars is located near the sun so that the electron temperature tends to be high.

6. Summary

Electron temperatures were studied in the dayside of two regions of (1) crustal-field region and (2) draped-field region using the LPW instrument onboard MAVEN focusing on the altitude region of 250–350 km. The LPW observations showed that the electron temperature was lower in the crustal-field region of strong magnetic field than in the draped field region at high altitudes. We suggest that electron and electron heat transport take place along magnetic field lines and that this transports heat in the ionosphere more effectively for crustal field geometries, where the field is more radial. But the conduction formalism needs more investigation for crustal fields due to kinetic effects including the greater importance of the balance between mirror force and the ambipolar electric field. The magnetic mirror force can transport electrons from the lower ionosphere where the cold electrons are dominant to higher altitudes, contributing to the electron

cooling, while the ambipolar electric field slows down the electron's upward motion. The solar EUV also affects the electron temperature, and the electron temperature is higher in the high EUV irradiances. It might be associated with the EUV energy deposition suggested by Peterson et al. (2018). The EUV irradiances are high around the perihelion and low around the aphelion, meaning that the electron temperature probably depends on the solar longitude.

Our data analysis shows that current models of the electron energetics (i.e., temperature) cannot accurately predict electron temperature above 250-km altitude in the crustal-field region, and this suggests that models need to take into account kinetic effects such as the mirror forces and ambipolar electric fields, among others. Magnetic mirror forces and ambipolar electric field can influence the electron heat conduction associated with a photoelectron transport in the crustal-field region where the local magnetic field is more vertical. These effects need to be considered in the crustal-field region because the electron mean free path exceeds the relevant length scale of temperature gradient, resulting in that the standard Spitzer conductivity cannot be applied. These processes have not been investigated in detail via modeling yet, and thus, properly accounting for these kinetic effects on the electron temperature in the crustal-field region should be a focus in future numerical simulations.

Acknowledgments
MAVEN data are publicly available through the Planetary Data System at https://pds-ppi.igpp.ucla.edu. This work was supported by Grant-in-Aid for Scientific Research (A) 16H02229 and Fostering Joint International Research (B) 18KK0093 from JSPS; NASA MAVEN Mission contract NNH10CC04C to the University of Colorado and a subcontract to the University of Kansas; and the French space agency CNES for the observations obtained with the SWEA instrument. The MAVEN project is supported by NASA through the Mars Exploration Program. The authors thank John Connerney for his advice on ionospheric magnetic fields.

References

Acuña, M. H. (1998). Magnetic field and plasma observations at Mars: Initial results of the Mars Global Surveyor mission. *Science*, *279*(5357), 1676–1680. https://doi.org/10.1126/science.279.5357.1676

Andersson, L., Ergun, R. E., Delory, G. T., Eriksson, A., Westfall, J., Reed, H., et al. (2015). The Langmuir Probe and Waves (LPW) instrument for MAVEN. *Space Science Reviews*, *195*(1-4), 173–198. https://doi.org/10.1007/s11214-015-0194-3

Andrews, D. J., Andersson, L., Delory, G. T., Ergun, R. E., Eriksson, A. I., Fowler, C. M., et al. (2015). Ionospheric plasma density variations observed at Mars by MAVEN/LPW. *Geophysical Research Letters*, *42*, 8862–8869. https://doi.org/10.1002/2015GL065241

Andrews, D. J., Opgenoorth, H. J., Edberg, N. J. T., André, M., Fränz, M., Dubinin, E., et al. (2013). Determination of local plasma densities with the MARSIS radar: Asymmetries in the high-altitude Martian ionosphere. *Journal of Geophysical Research: Space Physics*, *118*, 6228–6242. https://doi.org/10.1002/jgra.50593

Bertucci, C., Mazelle, C., Crider, D. H., Vignes, D., Acuña, M. H., Mitchell, D. L., et al. (2003). Magnetic field draping enhancement at the Martian magnetic pileup boundary from Mars Global Surveyor observations. *Geophysical Research Letters*, *30*(2), 1099. https://doi.org/10.1029/2002GL015713

Brain, D. A., Bagenal, F., Acuña, M. H., & Connerney, J. E. P. (2003). Martian magnetic morphology: Contributions from the solar wind and crust. *Journal of Geophysical Research*, *108*(A12), 1424. https://doi.org/10.1029/2002JA009482

Brain, D. A., Lillis, R. J., Mitchell, D. L., Halekas, J. S., & Lin, R. P. (2007). Electron pitch angle distributions as indicators of magnetic field topology near Mars. *Journal of Geophysical Research*, *112*, A09201. https://doi.org/10.1029/2007JA012435

Cain, J. C., Ferguson, B. B., & Mozzoni, D. (2003). An n=90 internal potential function of the Martian crustal magnetic field. *Journal of Geophysical Research*, *108*(E2), 5008. https://doi.org/10.1029/2000JE001487

Chamberlin, P. C., Woods, T. N., & Eparvier, F. G. (2007). Flare Irradiance Spectral Model (FISM): Daily component algorithms and results. *Space Weather*, *5*, S07005. https://doi.org/10.1029/2007SW000316

Chen, R. H., Cravens, T. E., & Nagy, A. F. (1978). The Martian ionosphere in light of the Viking observations. *Journal of Geophysical Research*, *83*(A8), 3871–3876. https://doi.org/10.1029/JA083iA08p03871

Choi, Y. W., Kim, J., Min, K. W., Nagy, A. F., & Oyama, K. I. (1998). Effect of the magnetic field on the energetics of Mars ionosphere. *Geophysical Research Letters*, *25*(14), 2753–2756. https://doi.org/10.1029/98GL51839

Coates, A. J., Tsang, S. M. E., Wellbrock, A., Frahm, R. A., Winningham, J. D., Barabash, S., et al. (2011). Ionospheric photoelectrons: Comparing Venus, Earth, Mars and Titan. *Planetary and Space Science*, *59*(10), 1019–1027. https://doi.org/10.1016/j.pss.2010.07.016

Connerney, J. E. P., Acuña, M. H., Ness, N. F., Kletetschka, G., Mitchell, D. L., Lin, R. P., & Reme, H. (2005). Tectonic implications of Mars crustal magnetism. *Proceedings of the National Academy of Sciences of the United States of America*, *102*(42), 14,970–14,975. https://doi.org/10.1073/pnas.0507469102

Cravens, T. E. (1997). *Physics of solar system plasmas*. Cambridge, UK: Cambridge University Press. https://doi.org/10.1017/CBO9780511529467

Cravens, T. E., Gombosi, T. I., Kozyra, J., Nagy, A. F., Brace, L. H., & Knudsen, W. C. (1980). Model calculations of the dayside ionosphere of Venus: Energetics. *Journal of Geophysical Research*, *85*(A13), 7778–7786. https://doi.org/10.1029/JA085iA13p07778

Cravens, T. E., Rahmati, A., Fox, J. L., Lillis, R., Bougher, S., Luhmann, J., et al. (2017). Hot oxygen escape from Mars: Simple scaling with solar EUV irradienace. *Journal of Geophysical Research: Space Physics*, *122*, 1102–1116. https://doi.org/10.1002/2016JA023461

Eparvier, F. G., Chamberlin, P. C., Wodds, T. N., & Thiemann, E. M. B. (2015). The solar extreme ultraviolet monitor for MAVEN. *Space Science Reviews*, *195*(1-4), 293–301. https://doi.org/10.1007/s11214-0150195-2

Ergun, R. E., Andersson, L., Peterson, W. K., Brain, D., Delory, G. T., Mitchell, D. L., et al. (2006). Role of plasma waves in Mars' atmospheric loss. *Geophysical Research Letters*, *33*, L14103. https://doi.org/10.1029/2006GL025785

Ergun, R. E., Morooka, M. W., Andersson, L. A., Fowler, C. M., Delory, G. T., Andrews, D. J., et al. (2015). Dayside electron temperature and density profiles at Mars: First results from the MAVEN Langmuir probe and waves instrument. *Geophysical Research Letters*, *42*, 8846–8853. https://doi.org/10.1002/2015GL065280

Fang, X., Luhmann, J. G., Ma, Y., Nagy, A. F., Dong, Y., Halekas, J. S., et al. (2017). Mars crustal magnetic fields and large-scale dayside ionospheric anomaly. Paper presented at American Geophysical Union Fall Meeting 2017, American Geophysical Union, New Orleans, LA.

Flynn, C. L., Vogt, M. F., Withers, P., Andersson, L., England, S., & Liu, G. (2017). MAVEN observations of the effects of crustal magnetic fields on electron density and temperature in the Martian dayside ionosphere. *Geophysical Research Letters*, *44*, 10,812–10,821. https://doi.org/10.1002/2017GL075367

Fowler, C. M., Andersson, L., Halekas, J., Espley, J. R., Mazelle, C., Coughlin, E. R., et al. (2017). Electric and magnetic variations in the near-Mars environment. *Journal of Geophysical Research: Space Physics*, *122*, 8536–8559. https://doi.org/10.1002/2016JA023411

Frahm, R. A., Winningham, J. D., Sharber, J. R., Scherrer, J. R., Jeffers, S. J., Coates, A. J., et al. (2006). Carbon dioxide photoelectron energy peaks at Mars. *Icarus*, *182*(2), 371–382. https://doi.org/10.1016/j.icarus.2006.01.014

Hanson, W. B., & Mantas, G. P. (1988). Viking electron temperature measurements: Evidence of a magnetic field in the Martian ionosphere. *Journal of Geophysical Research*, *93*(A7), 7538–7544. https://doi.org/10.1029/JA093iA07p07538

Jakosky, B. M., Lin, R. P., Grebowsky, J. M., Luhmann, J. G., Mitchell, D. F., Beutelschies, G., et al. (2015). The Mars Atmosphere and Volatile Evolution (MAVEN) mission. *Space Science Reviews*, *195*(1-4), 3–48. https://doi.org/10.1007/s11214-015-0139-x

Johnson, R. E. (1978). Comment on ion and electron temperatures in the Martian upper atmosphere. *Geophysical Research Letters*, *5*(11), 989–992. https://doi.org/10.1029/GL005i011p00989

Liemohn, M. W., Frahm, R. A., Winningham, J. D., Ma, Y., Barabash, S., Lundin, R., et al. (2006). Numerical interpretation of high-altitude photoelectron observations. *Icarus*, *182*(2), 383–395. https://doi.org/10.1016/j.icarus.2005.10.036

Liemohn, M. W., Mitchell, D. L., Nagy, A. F., Fox, J. L., Reimer, T. W., & Ma, Y. (2003). Comparisons of electron fluxes measured in the crustal fields at Mars by the MGS magnetometer/electron reflectometer instrument with a B field-dependent transport code. *Journal of Geophysical Research*, *108*(E12), 5134. https://doi.org/10.1029/2003JE002158

Lillis, R. J., Brain, D. A., Bougher, S. W., Leblanc, F., Luhmann, J. G., Jakosky, B. M., et al. (2015). Characterizing atmospheric escape from Mars today and through time, with MAVEN. *Space Science Reviews*, *195*(1-4), 357–422. https://doi.org/10.1007/s11214-015-0165-8

Lundin,, R., Barabash, S., Andersson, H., Holmström, M., Grigoriev, A., Yamauchi, M., et al. (2004). Solar wind-induced atmospheric erosion at Mars: First results from ASPERA-3 on Mars Express. *Science*, *305*(5692), 1933–1936. https://doi.org/10.1126/science.1101860

Matta, M., Galand, M., Moore, L., Mendillo, M., & Withers, P. (2014). Numerical simulations of ions and electron temperatures in the ionosphere of Mars: Multiple ions and diurnal variations. *Icarus*, *227*, 78–88. https://doi.org/10.1016/j.icarus.2013.09.006

Mitchell, D. L., Lin, R. P., Rème, H., Crider, D. H., Cloutier, P. A., Connerney, J. E. P., et al. (2000). Oxygen auger electrons observed in Mars' ionosphere. *Geophysical Research Letters*, *27*(13), 1871–1874. https://doi.org/10.1029/1999GL010754

Mitchell, D. L., Mazelle, C., Sauvaud, J. A., Thocaven, J. J., Rouzaud, J., Fedorov, A., et al. (2016). The MAVEN Solar Wind Electron Analyzer. *Space Science Reviews*, *200*(1-4), 495–528. https://doi.org/10.1007/s11214-015-0232-1

Peterson, W. K., Fowler, C. M., Andersson, L. A., Thiemann, E. M. B., Jain, S. K., Mayyasi, M., et al. (2018). Martian electron temperatures in the subsolar region: MAVEN observations compared to a one-dimensional model. *Journal of Geophysical Research: Space Physics*, *123*, 5960–5973. https://doi.org/10.1029/2018JA025406

Rees, M. H. (1989). *Physics and chemistry of the upper atmosphere*. Cambridge, UK: Cambridge University Press. https://doi.org/10.1017/CBO9780511573118

Rohrbaugh, R. P., Nisbet, J. S., Bleuler, E., & Herman, J. R. (1979). The effect of energetically produced O_2^+ on the ion temperatures of the Martian thermosphere. *Journal of Geophysical Research*, *84*(A7), 3327–3338. https://doi.org/10.1029/JA084iA07p03327

Sakai, S., Andersson, L., Cravens, T. E., Mitchell, D. L., Mazelle, C., Rahmati, A., et al. (2016). Electron energetics in the Martian dayside ionosphere: Model comparisons with MAVEN data. *Journal of Geophysical Research: Space Physics*, *121*, 7049–7066. https://doi.org/10.1002/2016JA022782

Sakai, S., Rahmati, A., Mitchell, D. L., Cravens, T. E., Bougher, S. W., Mazelle, C., et al. (2015). Model insights into energetic photoelectrons measured at Mars by MAVEN. *Geophysical Research Letters*, *42*, 8894–8900. https://doi.org/10.1002/2015GL065169

Schunk, R. W., & Nagy, A. F. (2009). *Ionospheres: Physics, Plasma Physics, and Chemistry* (2nd ed.). Cambridge, UK: Cambridge University Press. https://doi.org/10.1017/CBO9780511635342

Singhal, R. P., & Whitten, R. C. (1988). Thermal structure of the ionosphere of Mars: Simulations with one- and two-dimensional models. *Icarus*, *74*(2), 357–364. https://doi.org/10.1016/0019-1035(88)90048-6

Thiemann, E. M. B., Chamberlin, P. C., Eparvier, F. G., Templeman, B., Woods, T. N., Bougher, S. W., & Jakosky, B. M. (2017). The MAVEN EUVM model of solar spectral irradiance variability at Mars: Algorithms and results. *Journal of Geophysical Research: Space Physics*, *122*, 2748–2767. https://doi.org/10.1002/2016JA023512

Withers, P., Mendillo, M., Rishbeth, H., Hinson, D. P., & Arkani-Hamed, J. (2005). Ionospheric characteristics above Martian crustal magnetic anomalies. *Geophysical Research Letters*, *32*, L16204. https://doi.org/10.1029/2005GL023483

Xu, S., Mitchell, D., Liemohn, M., Fang, X., Ma, Y., Luhmann, J., et al. (2017). Martian low-altitude magnetic topology deduced from MAVEN/SWEA observations. *Journal of Geophysical Research: Space Physics*, *122*, 1831–1852. https://doi.org/10.1002/2016JA023467